

## Neutron reflectivity measurements of the translational motion of tris(naphthylbenzene) at the glass transition temperature

Stephen F. Swallen, Marie K. Mapes, Yong Seol Kim,  
Robert J. McMahon, and M. D. Ediger<sup>a)</sup>

*Department of Chemistry, University of Wisconsin-Madison, Madison, Wisconsin 53706*

Sushil Satija

*NIST Center for Neutron Research, National Institute of Standards and Technology,  
Gaithersburg, Maryland 20899*

(Received 25 October 2005; accepted 9 March 2005; published online 8 May 2006)

The translational dynamics of the low molecular weight glass-former tris(naphthylbenzene) have been studied on the length scale of a few nanometers at the glass transition temperature  $T_g$ . Neutron reflectivity was used to measure isotopic interdiffusion of multilayer samples created by physical vapor deposition. Deposition with the substrate held at  $T_g - 6$  K allows observation of dynamics characterizing the equilibrium supercooled liquid. The diffusion coefficient measured at  $q = 0.03 \text{ \AA}^{-1}$  was determined to be  $1 \times 10^{-17} \text{ cm}^2/\text{s}$  at 342 K ( $T_g$ ). The self-part of the intermediate scattering function  $I_s(q, t)$  decays exponentially. Samples deposited well below  $T_g$  show a substantial thermal history effect during subsequent translational motion at  $T_g$ . © 2006 American Institute of Physics. [DOI: 10.1063/1.2191492]

### INTRODUCTION

In the past 20 years, significant advances have been made in our understanding of dynamics in supercooled liquids and glasses.<sup>1-3</sup> New theoretical approaches,<sup>4-7</sup> and particularly the application of mode-coupling theory,<sup>8-10</sup> have spurred further experimental and simulation work. Powerful simulations have probed microscopic aspects of the dynamics, at least for moderately supercooled liquids.<sup>11-16</sup> New experimental techniques, including single molecule spectroscopy,<sup>17</sup> dynamic hole-burning methods,<sup>18</sup> dielectric fluctuation spectroscopy,<sup>19</sup> multidimensional solid-state NMR methods,<sup>20,21</sup> and solvation dynamics<sup>22</sup> have been used to interrogate dynamics near the glass transition temperature  $T_g$  and provided insights not previously available.

One of the most interesting recent developments is the understanding that the dynamics near  $T_g$  are spatially heterogeneous in at least some glass-forming systems.<sup>22-24</sup> Even for a single component liquid in a single thermodynamic phase, the dynamics of molecules in one region can be orders of magnitude faster or slower than the dynamics of molecules only a few nanometers away. Almost all of the direct information that we have about spatially heterogeneous dynamics comes from experiments that are sensitive to the reorientation of molecules.<sup>22-24</sup> For translational motion, we know that diffusion coefficients measured on large length scales in deeply supercooled liquids are unusually large as compared to reorientation times or the viscosity, and this is thought to be a consequence of heterogeneous dynamics.<sup>25,26</sup> However, existing measurements of translational dynamics in supercooled liquids do not have spatial resolution at the single nanometer length scale and so the direct observation

of the effect of heterogeneity on translational diffusion has so far been limited to a few studies of probe motion in polymeric glass formers.<sup>27-29</sup> In these systems, the effects of heterogeneity on translational motion are apparently so large that they persist even for measurements performed with a resolution of 150 nm.

Neutron scattering provides an elegant method to learn about translational motion on the nanometer length scale. The neutron wavelength is short ( $\lambda \sim 1$  nm) and a much better match to the length scale of interest than the optical radiation ( $\lambda \sim 500$  nm) used to study the translational motion of dye molecules. Neutron scattering from protons is very different from scattering from deuterons, providing an almost perturbation-free method for labeling certain molecules. Thus neutron scattering can provide information about self-motion (to an excellent approximation) whereas optical methods are limited to probe motion. Dynamic neutron experiments [quasielastic neutron scattering (QENS) and neutron spin echo (NSE)] have been used extensively to study translational motion in supercooled liquids; see, for example, Refs. 30 and 31. Unfortunately, these methods are limited at present to time scales of 100 ns or less, and thus are not yet useful to study translational motion near  $T_g$ .

Static neutron scattering methods, such as neutron reflectivity, can be used to study very slow diffusion if a suitable sample can be constructed with a sharp boundary between layers of deuterio and protio molecules.<sup>32,33</sup> Changes in the scattering curve with time can be related to changes in the composition profile. For neutron studies, a particularly useful experiment is to construct a structure that is isotopically periodic (the concentration of protio/deuterio material varies regularly throughout the sample) but otherwise chemically homogeneous.<sup>33</sup> Conceptually, this structure is useful because the motion of the molecules should be very similar

<sup>a)</sup>Electronic mail: ediger@chem.wisc.edu

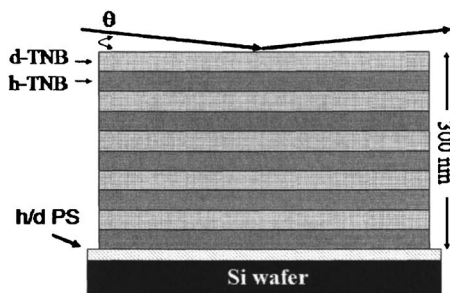


FIG. 1. Schematic representation of multilayer samples created by physical vapor deposition. Each of the ten layers is 30 nm thick, with alternating *h*-TNB/*d*-TNB layers. A 10 nm *h/d* polystyrene film was spin coated on the silicon wafer prior to vapor deposition. The neutron beam was incident to the sample surface at angle  $\theta$ .

in such a sample to motion in a bulk sample with no isotopic labeling or nearby interfaces. Practically, such samples give rise to strong diffraction peaks and the decay of these peaks with time provides direct information about translational motion at a well-defined wavelength. This type of experiment has previously been utilized to study translational motion in polymers,<sup>33</sup> metallic glass formers,<sup>34,35</sup> and other systems<sup>34</sup> (in these latter cases, isotopes such as <sup>57</sup>Fe and <sup>10</sup>B were used).

Here we report, for the first time, the translational dynamics of a low molecular weight organic glass former at  $T_g$  with nanometer resolution. We have studied tris(naphthylbenzene) (TNB), a typical fragile glass former. We use neutron reflectivity measurements as described in the previous paragraph. Multilayer samples of protio and deuterio TNB were prepared by physical vapor deposition, as illustrated schematically in Fig. 1. Initially, the interfaces between *h*-TNB and *d*-TNB layers are quite sharp and multiple diffraction peaks are observed in the neutron reflectivity. Stated simply, the idea of this experiment is that the neutrons see the stripes in Fig. 1 but the molecules do not.

By following the time decay of the diffraction peaks at particular wave vectors, we have determined the diffusion coefficient for TNB at  $T_g$  (342 K) at wave vectors of 0.03 and 0.05  $\text{\AA}^{-1}$ . We show that the amplitude of *h*-TNB/*d*-TNB concentration variations at  $q=0.03 \text{\AA}^{-1}$  decays exponentially in time (or very nearly so). Additionally, we show that any isotope effects in these experiments are very small. A surprising aspect of these experiments is that the observed translational motion depends sensitively on the substrate temperature during vapor deposition. We argue that the deposition within a few degrees of  $T_g$  produces samples that are in the equilibrium supercooled liquid state; deposition at lower temperatures produces samples in which diffusion shows a strong dependence on thermal history. The diffusion coefficients reported here on the 5 nm length scale are about ten times smaller than values previously reported for TNB (Ref. 25) at  $T_g$  on longer length scales. This could indicate that TNB molecules translate large distances before Fickian diffusion is an accurate description. We will report the wave vector dependence of the diffusion coefficient over a range of wave vectors in a future publication.

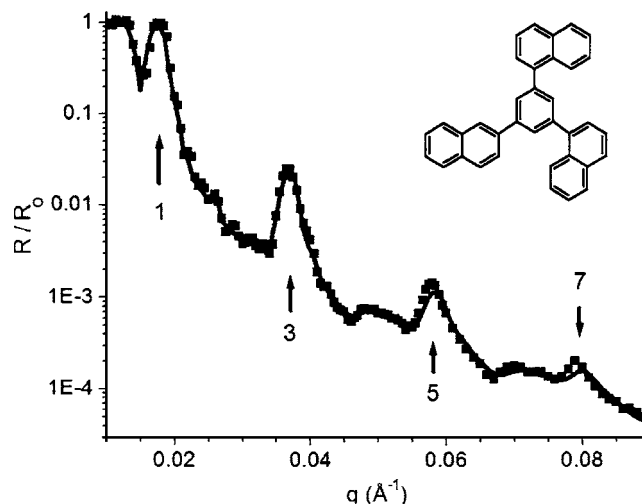


FIG. 2. Neutron reflectivity data for an unannealed multilayer sample (symbols) and fit (solid line) found using REFLFIT. The numbers indicate the harmonic peaks in the reflectivity due to the periodic sample structure. The inset shows the structure of 1,3-bis(1-naphthyl)-5-(2-naphthyl)benzene (TNB).

## EXPERIMENTAL TECHNIQUE

1,3-bis(1-naphthyl)-5-(2-naphthyl)benzene, more commonly known as  $\alpha\alpha\beta$ -TNB or tris(naphthylbenzene), was prepared as described previously.<sup>36</sup> The structure is shown as an inset in Fig. 2. A partially deuterated isomer was also synthesized, in which the 14 sites on the two 1-naphthyl groups were isotopically substituted. The protio and deuterio versions of tris(naphthylbenzene) will be subsequently referred to as *h*-TNB and *d*-TNB, respectively. Note that the literature prior to 1996 contains several papers characterizing a substance identified as 1,3,5-tri- $\alpha$ -naphthylbenzene. Whitaker and McMahon established that these earlier studies were almost certainly performed on  $\alpha\alpha\beta$ -TNB.<sup>36</sup>

Physical vapor deposition was used to create multilayer thin films of *h*-TNB and *d*-TNB. Samples were deposited onto 76 mm diameter, 3 mm thick silicon wafers (Wafer World and Virginia Semiconductor). The silicon was used as received, with the native oxide coating. The deposition rate was typically 0.15 nm/s. The substrate temperature was held constant during deposition (ranging from 322 to 339 K) using a Lakeshore 340 controller with platinum RTD sensors. Prior to deposition, the substrate was spin coated with a 10 nm polystyrene layer (Polymer Source,  $\sim 10^6$  g/mol), which acted to minimize the crystallization and dewetting of the TNB film during annealing. The polystyrene was a mixture of protio and perdeuterio chains, in order to approximately match the neutron scattering length density of the first protio TNB layer. Following deposition, the samples were slowly cooled and held at room temperature for one to five days before being annealed near  $T_g$ .

The multilayer samples used in the neutron reflectivity measurements were constructed with each layer nominally 30 nm thick and a total of ten layers in each sample (see Fig. 1). This created a periodic structure with a fundamental wavelength of 60 nm (the thickness of a single *h*-TNB/*d*-TNB bilayer). The thickness of each layer was measured during deposition using a quartz crystal microbalance. After

preparation, the total sample thickness was measured by ellipsometry and found to agree well with the sum of the individual layer thicknesses. The precise thickness of each layer was determined by fits to the neutron reflectivity measurements on the as-prepared samples. Values from the reflectivity agreed with the quartz crystal microbalance measurements within about 5%.

Due to the geometry of the vapor deposition apparatus, the samples were created with a slight radial thickness gradient; the thickness in the 5 cm region probed by the neutron beam varied by 2%. This thickness gradient slightly blurs the initial concentration profile extracted from the neutron reflectivity data, but causes a negligible error in the reported diffusion coefficients.

The vapor deposition process created a very smooth top surface, with typically less than 1 nm of surface roughness.<sup>37</sup> This was determined by measurements of the top surface using atomic force microscopy (AFM) and fits to neutron reflectivity data on single layer TNB samples.

Thermal analysis was used to verify that vapor deposition did not chemically alter TNB. Differential scanning calorimetry (DSC) of TNB directly deposited into a DSC pan gave the same melting point as DSC experiments on TNB that had not been vapor deposited. Both melting points were in good agreement with the literature value.<sup>36</sup>

Neutron reflectivity experiments were conducted at the NIST Center for Neutron Research at the National Institute of Standards and Technology (NCNR-NIST). The NG7 horizontal reflectometer utilized a 4.76 Å collimated neutron beam, with a wavelength divergence of 0.18 Å. The angular divergence of the beam was varied through the reflectivity scan and this provided a relative  $q$  resolution  $\Delta q/q=0.04$  ( $q=4\pi\sin\theta/\lambda$ , where  $\theta$  is the incident and final angle with respect to the surface of the film, as shown in Fig. 1). Reflectivity measurements were performed during annealing by placing the sample into an in-line oven at the glass transition temperature  $T_g=342.0$  K. The temperature was held constant to within  $\pm 0.1$  K during the annealing process, which ranged up to 30 h. Scans were made over a  $q$  range from 0.01 Å<sup>-1</sup> to a maximum of 0.13 Å<sup>-1</sup>, with a typical duration of 30 min/scan.

The nanometer resolution of these experiments results from the small neutron wavelength and strong difference in neutron scattering from protons and deuterons. The scattering length densities for  $h$ -TNB ( $2.35\times 10^{-6}$  Å<sup>-2</sup>),  $d$ -TNB ( $4.65\times 10^{-6}$  Å<sup>-2</sup>), and  $h/d$  polystyrene ( $2.2\times 10^{-6}$  Å<sup>-2</sup>) have been calculated based upon the known density and chemical composition, and the values for silicon oxide ( $3.45\times 10^{-6}$  Å<sup>-2</sup>) and silicon ( $2.07\times 10^{-6}$  Å<sup>-2</sup>) were obtained from the literature; these values are fixed during the analysis of the neutron reflectivity data. An analysis software package called REFLFIT, provided by NIST, was used to analyze the neutron reflectivity data.

## RESULTS

*Structure of as-prepared samples.* Figure 1 shows the nominal structure of the samples studied by neutron reflectivity. As described above, the samples were prepared by

vapor deposition of protio and deuterio tris(naphthylbenzene). A typical neutron reflectivity curve for a  $h$ -TNB/ $d$ -TNB multilayer is shown in Fig. 2. This sample was deposited at  $T_g-6$  K, and was held at room temperature during this measurement without having been annealed. Multilayer structures give rise to a constructive interference pattern at wave vectors  $q$  related to the layer thicknesses. In this case, since the interfaces between the  $h$ -TNB and  $d$ -TNB layers are relatively sharp, multiple diffraction peaks (Bragg peaks) are observed. For a perfect sample in which every TNB layer has the same thickness, as shown in Fig. 1, only odd harmonics should be observed (since the Fourier series for a square wave contains only odd terms). Figure 2 shows strong peaks for the fundamental reflection and the third and fifth harmonics, while the even harmonics are barely visible.

The particular  $q$  values at which diffraction peaks occur is determined by the TNB layer thicknesses. Since the fundamental wavelength  $\lambda$  of these samples is about 60 nm, and  $q$  is related to  $\lambda$  by  $q=2\pi/\lambda$ , one might naively expect the fundamental peak to occur at  $q\sim 0.010$  Å<sup>-1</sup>. Because the critical edge of Si occurs at  $q=0.013$  Å<sup>-1</sup>, all the diffraction peaks are shifted to higher values of  $q$ , and the fundamental peak occurs at 0.017 Å<sup>-1</sup>. This shift is negligible for the seventh and higher harmonics, allowing the lower harmonic peaks to be shifted to a corrected wave vector (denoted as  $q'$ ) for subsequent analysis. For describing dynamics at particular length scales, these corrected  $q'$  values (which are indicative of the actual length scale in the sample) will be used throughout the remainder of this paper. In Fig. 2,  $q'$  values for the first, third, and fifth harmonics are 0.011, 0.035, and 0.058 Å<sup>-1</sup>, respectively, corresponding to wavelengths of 55, 18, and 11 nm.

The program REFLFIT was used to find the best fit to the neutron reflectivity data presented in Fig. 2 (shown as solid line). In this fitting procedure, the scattering length density (SLD) of each layer was fixed at the calculated values for pure  $h$ -TNB,  $d$ -TNB,  $h/d$  polystyrene, silicon oxide, and silicon. The overall structure of the multilayer sample was specified but the fitting program was free to adjust the thickness of each layer, the width of each interface, and the top surface roughness, in order to minimize the sum of the residuals. The scattering length density (SLD) profile of the multilayer sample corresponding to this calculated reflectivity curve is shown in Fig. 3. The  $d$ -TNB/air interface is on the left, while the polystyrene and silicon oxide layers and the silicon substrate are at the greatest depth, near 300 nm. This plot of SLD is directly and linearly related to the concentration profile of  $h$ -TNB and  $d$ -TNB in the sample. Although the vapor deposition process produces surfaces with subnanometer flatness, our samples deposited at  $T_g-6$  K were observed to have  $h$ -TNB/ $d$ -TNB interfacial widths of roughly 4 nm. This presumably is due to translational motion that takes place during the roughly 2 h required for the deposition process.

Some readers might find the analogy between this experiment and an optical transmission grating to be helpful. If a glass slide has periodic stripes of metal deposited on it (e.g., a Ronchi ruling), a laser beam passing through the pattern will give rise to a series of diffraction peaks, with the

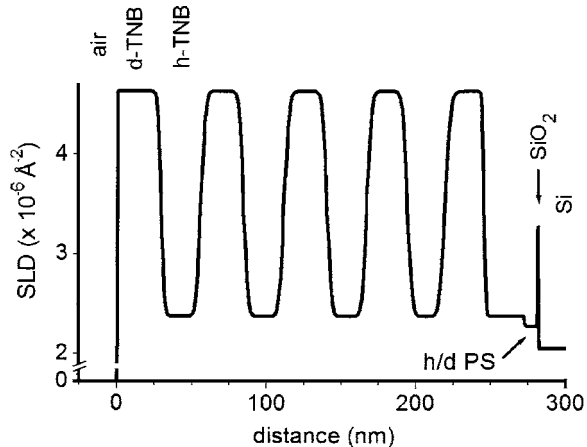


FIG. 3. The scattering length density (SLD) profile which provided the best fit to the data presented in Fig. 2. The sample is composed of five repeating *h*-TNB/*d*-TNB bilayers, on a 10 nm polystyrene film spin coated onto a silicon wafer with native oxide coating. The TNB portion of the SLD profile is linearly related to the concentration profile.

higher order peaks being less intense. If the width of the metal stripes matches the width of the gap between them, the diffraction pattern will contain only odd harmonics (as in Fig. 2). The index of refraction for light is analogous to the scattering length density for neutrons.

#### Evolution of the composition profile during annealing.

Following the measurement of the unannealed samples at room temperature, each sample was annealed at 342 K in a specially constructed oven which allowed real time neutron reflectivity measurements. The time series for one multilayer is shown in Fig. 4. The Bragg peaks decrease in intensity due to translational diffusion which further blurs the interfaces between *h*-TNB and *d*-TNB. The time evolution of the entire reflectivity curves, and, in particular, the decay rates of each Bragg peak, provides the data necessary to determine the evolution of the composition in the multilayer samples during the annealing process.

As a first step toward understanding the dynamics of

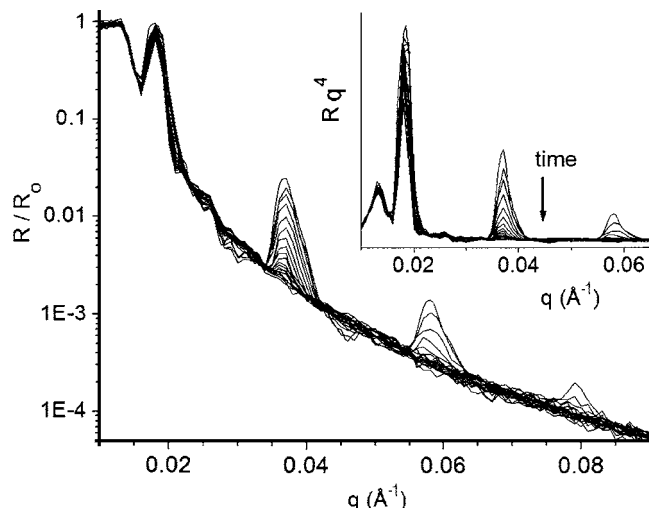


FIG. 4. Neutron reflectivity data for a multilayer sample while annealing at  $T_a=342$  K. Each data set required about 30 min to scan from  $q=0.01$  to  $0.09 \text{ \AA}^{-1}$ . The inset is the same set of data after multiplying each curve by  $q^4$  which removes the  $q$ -dependent base line.

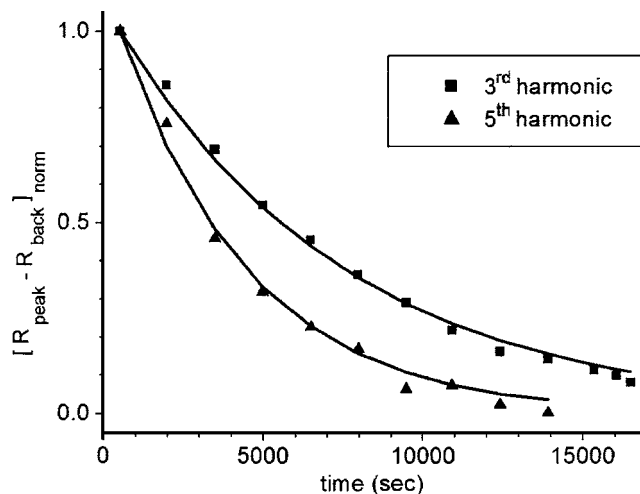


FIG. 5. Normalized Bragg peak intensity as a function of time for a multilayer sample. As indicated by Eq. (3), this function is approximately equal to the square of the self-part of the intermediate scattering function  $I_s(q, t)$ . Solid lines are exponential fits to data for the third (squares) and fifth (triangles) harmonics.

TNB in these multilayer samples, translational motion was assumed to occur by Fickian diffusion. This has been shown to be a good description of dynamics in many high temperature liquids and for TNB even somewhat below the melting point.<sup>38</sup> For Fickian diffusion, the diffusion coefficient  $D$  is invariant with distance or wave vector and the mean square displacement is linear in time for all times. For Fickian diffusion, the amplitude of a composition wave with any  $q$  decays exponentially with a time constant that depends upon  $q$  and  $D$ :

$$S(q, t)/S(q, 0) = \exp(-q^2 D t). \quad (1)$$

In an isotopically labeled system, if the dynamics and thermodynamics are not affected by labeling, this function is equivalent to the self-part of the intermediate scattering function, that is,

$$I_s(q, t)/I_s(q, 0) = S(q, t)/S(q, 0). \quad (2)$$

For an infinitely periodic system which is accurately described in the single scattering approximation,<sup>39</sup> these functions can be measured directly from the intensity of Bragg peaks like those shown in Fig. 4,<sup>35</sup>

$$\begin{aligned} \left[ \frac{I_s(q, t)}{I_s(q, t=0)} \right]^2 &\approx \left[ \frac{R_{\text{peak}} - R_{\text{background}}}{(R_{\text{peak}} - R_{\text{background}})_0} \right] \\ &= [R_{\text{peak}} - R_{\text{back}}]_{\text{norm}}. \end{aligned} \quad (3)$$

In practice, the format shown as an inset in Fig. 4 is useful for calculating this function; multiplying the reflectivity curve times  $q^4$  removes that part of the signal that comes from reflection from any sharp interface.

Figure 5 shows the normalized peak intensities of the third and fifth harmonic peaks following subtraction of the background, for a typical multilayer sample. As expected from Eqs. (1)–(3), the data are reasonably described by an exponential decay. If the normalized peak intensity falls to  $1/e$  of its initial value in a time  $\tau$ , then the diffusion coefficient can be estimated by

$$D = \frac{1}{2q^2\tau}. \quad (4)$$

For the third harmonic at  $q' = 0.029 \text{ \AA}^{-1}$ , the measured  $\tau = 7300 \text{ s}$ , giving an estimated diffusion coefficient  $D \approx 8 \times 10^{-18} \text{ cm}^2/\text{s}$  at  $T_g$ . The fifth harmonic at  $q' = 0.048 \text{ \AA}^{-1}$  gives a value  $D \approx 5 \times 10^{-18} \text{ cm}^2/\text{s}$ .

The format of Fig. 5 is useful for a quick evaluation of the experimental data and for quantitatively comparing experiments on different samples. As we show below, the diffusion coefficients obtained at the third and fifth harmonics using Eq. (4) are in error by about 30%. Based on model calculations, we know that the approximation represented by Eq. (3) is somewhat inaccurate for our samples because only a small number of periods (five sets of bilayers) are present in our multilayers. Equation (3) cannot be used to study the time dependence of the fundamental reflection at  $q = 0.017 \text{ \AA}^{-1}$  because this reflection is saturated and thus the single scattering approximation is not appropriate.

*Prediction of neutron reflectivity during annealing.* A more accurate procedure for comparing the neutron reflectivity data to the predictions of the Fickian diffusion model (with a particular value for  $D$ ) is described in this section. (1) The reflectivity curve for the unannealed sample (or in some cases the first data set obtained during annealing) is fit using REFLFIT, and the SLD profile is extracted, as shown in Fig. 3. (2) The SLD profile for the TNB portion of the sample is converted to a concentration profile, using the calculated values for the SLD for pure *d*-TNB and *h*-TNB. This defines the composition profile at  $t=0$ . (3) The  $t=0$  composition profile is reflected and placed adjacent to itself, which imposes reflecting boundary conditions on the subsequent diffusion process. This profile is Fourier transformed as a periodic structure, then attenuated at every  $q$  for a particular  $t$  as indicated by Eq. (1). The resulting function is inverse-Fourier transformed and the reflected portion of the profile is removed; this defines the composition profile at time  $t$ . (4) The composition profile at  $t$  is converted back to a SLD profile and the SLD profile of the polystyrene, silicon oxide, and silicon are added. REFLFIT is used to calculate the neutron reflectivity curve from this SLD profile and this reflectivity curve is compared to the experimental data.

Figure 6 shows a comparison between a measured set of reflectivity curves and the curves calculated assuming Fickian diffusion. As described in the previous paragraph, the thick black curve is a *fit* to the data at  $t=0$ . The thin black lines are *predictions* using  $D = 1.0 \times 10^{-17} \text{ cm}^2/\text{s}$ . Clearly the predicted curves are in excellent agreement with the experimental data, particularly for the third harmonic ( $q \sim 0.03 \text{ \AA}^{-1}$ ). For this data set, a slightly different value of  $D$  produces a better fit for the fifth harmonic:  $D = 0.8 \times 10^{-17} \text{ cm}^2/\text{s}$  (not shown). Due to the saturation of the fundamental reflection, only the third and fifth harmonics provide reliable diffusion coefficients for these samples. A small difference between the optimal  $D$  values for the third and fifth harmonics was observed in several samples and will be discussed below.

*Does  $I_s(q,t)$  decay exponentially?* Essentially every measure of molecular motion in supercooled fragile liquids

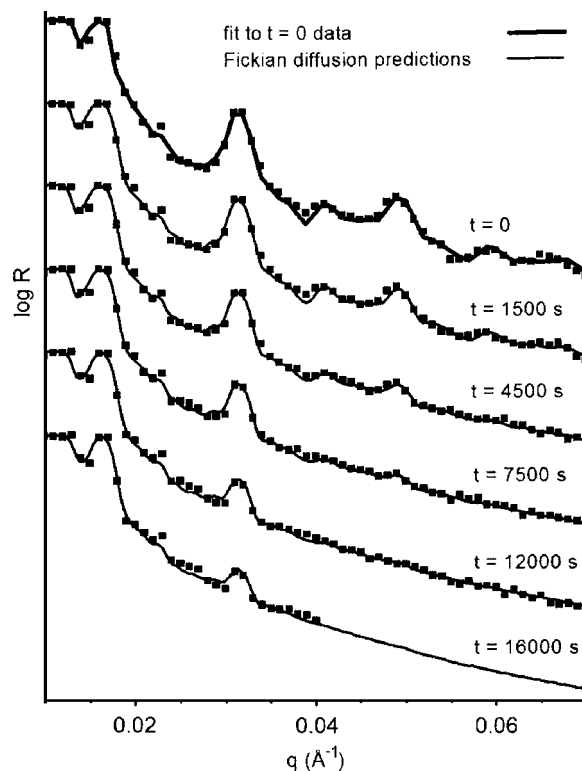


FIG. 6. Reflectivity data for an unannealed sample ( $t=0$ ) and at subsequent times during the annealing process at  $T_g$ . The thick solid line at  $t=0$  is the best fit, calculated using the REFLFIT program. Thinner solid lines at later times are predictions based on a Fickian model of diffusion, with a diffusion coefficient  $D = 1.0 \times 10^{-17} \text{ cm}^2/\text{s}$ .

has a nonexponential correlation function associated with it. For TNB in particular, dielectric relaxation,<sup>40</sup> photon correlation spectroscopy,<sup>41</sup> and NMR (Ref. 42) experiments agree that dynamics near  $T_g$  are well described by the Kohlrausch-Williams-Watts (KWW) function  $\exp[-(t/\tau)^\beta]$  with  $\beta=0.5$ . In contrast, the Fickian model of diffusion predicts an exponential decay of  $I_s(q,t)$  for all values of  $q$ . In reality, we expect that  $I_s(q,t)$  should decay exponentially at low  $q$  and nonexponentially at high  $q$ . Thus it is of interest to quantify the time dependence of  $I_s(q,t)$  in these experiments on TNB at  $T_g$ .

As described above, Fig. 6 compares experimental reflectivity curves with the predictions of Fickian diffusion. If we focus on the third harmonic, we see that the time dependence of this peak is described exceedingly well by the Fickian model in which  $I_s(q,t)$  decays exponentially ( $\beta=1$ ). In order to quantify how nonexponential  $I_s(q,t)$  could be and still be consistent with the experimental data, we present related comparisons in Figs. 7 and 8 using the same experimental data. For the calculations shown in Fig. 7,  $I_s(q,t)$  decays as a KWW function with  $\beta=0.5$ , while the calculations in Fig. 8 have  $\beta=0.7$ . Clearly the agreement between the experiment and calculation is better in Fig. 6 than in either Fig. 7 or 8, and on this basis we conclude that  $I_s(q,t)$  decays exponentially or nearly so. Quantitatively, these neutron reflectivity data are fully consistent with a  $\beta=1.0$ , but not with a value of  $\beta \leq 0.7$ . While there were some variations in the  $D$  values obtained for different samples (see discussion below), in every case, the time evolution was found to be exponential, or nearly so.

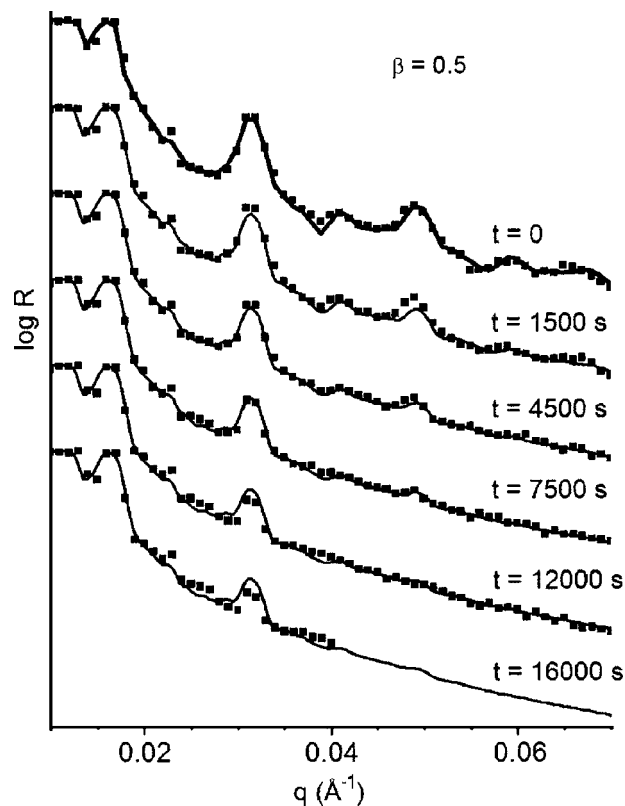


FIG. 7. The same reflectivity data as shown in Fig. 6. Thin solid lines are predictions with all parameters equal to those in Fig. 6, except that  $I_s(q, t)$  decays nonexponentially, with a KWW  $\beta=0.5$ .

**Reproducibility.** In order to test the reproducibility of these data, experiments have been repeated under the same deposition and annealing conditions. When two samples are prepared within a few days of each other, the observed diffusion is very similar. (The difference between the squares and triangles in Fig. 10 illustrates the typical agreement.) When two samples are prepared months apart, somewhat larger differences are observed. These differences are illustrated in Table I. For each of the three samples listed, we determined the best fit to the neutron reflectivity curves, optimizing the fit either for the third or fifth harmonic. For the third harmonic, fits that change  $D$  by 20% are easily distinguished, and for the fifth harmonic variations of 30% can be distinguished. In light of this, Table I indicates reasonable consistency among the different samples.

Variations in sample conditions such as silicon wafer substrate thickness or crystal orientation and the presence or absence of the underlying polystyrene layer were found to have no effect on the results. Generally, the TNB films began to crystallize during the annealing process. As determined by optical microscopy, crystallinity at the end of the annealing process varied from 0.2%–5%, with 2% being typical. We found no correlation between the level of crystallinity and the observed diffusion behavior.

**Effect of thermal history.** These experiments presented us with an interesting challenge. In order to produce samples with sharp interfaces between  $h$ -TNB and  $d$ -TNB, it is best to deposit the layers deep in the glassy state where no significant diffusion occurs during the 1–2 h required to pro-

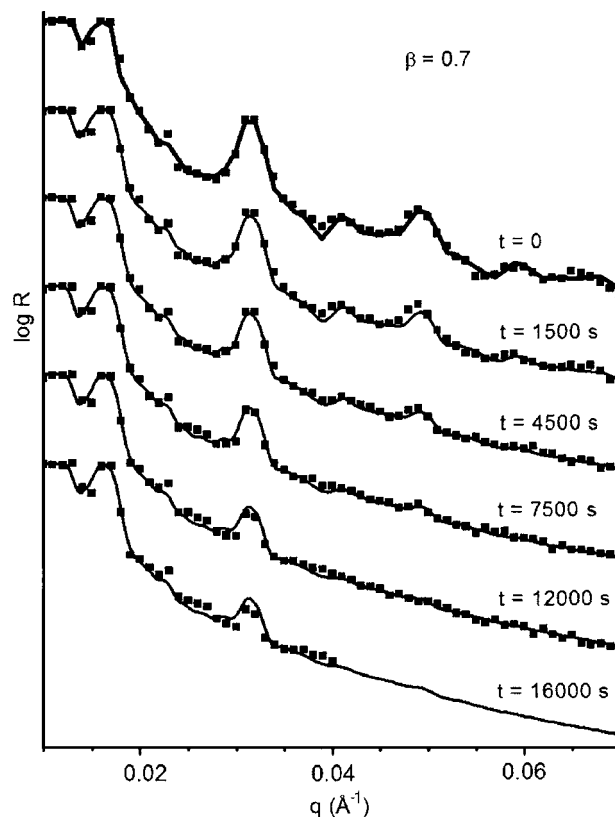


FIG. 8. The same reflectivity data as shown in Fig. 6. Thin solid lines are predictions with all parameters equal to those in Fig. 6, except that  $I_s(q, t)$  decays nonexponentially, with a KWW  $\beta=0.7$ . Clearly Fig. 6 represents a better fit to the data.

duce a multilayer sample. We observe that deposition at  $T_g - 20$  K produces considerably sharper diffraction peaks (not shown) than those produced by deposition at  $T_g - 6$  K (shown in Fig. 2). However, we found that deposition far below  $T_g$  produced samples far from equilibrium that showed substantial thermal history effects during their subsequent annealing at  $T_g$ . In this section, we show that deposition at  $T_g - 6$  K is a good compromise. We present evidence that diffusion during the subsequent annealing of such samples is independent of thermal history.

A series of multilayer samples was prepared by vapor depositing onto substrates held at temperatures ranging from  $T_g - 3$  to  $T_g - 20$  K. Figure 9 shows the normalized peak intensity function for the third harmonic observed during the annealing of these samples at  $T_g$ ; as described above, this function is directly related to  $I_s(q, t)$ . The sample deposited at  $T_g - 20$  K shows a long induction time, during which evolution of the concentration profile occurs only very slowly. Interestingly, this time is about  $40\tau_\alpha$ , where  $\tau_\alpha$  is the structural relaxation time at  $T_g$ .<sup>40</sup> Samples deposited at or above  $T_g - 12$  K are very different from the  $T_g - 20$  K sample and are very similar to each other. We interpret the difference between the  $T_g - 12$  K curve and the  $T_g - 6$  K curve as just barely significant. The difference between the  $T_g - 6$  K and  $T_g - 3$  K curves is not significant given the larger uncertainty in the latter data set and because Eq. (3) is a worse approximation for the  $T_g - 3$  K curve. (Both of these follow because the initial peak amplitude was smaller in the  $T_g - 3$  K data).

TABLE I. Diffusion coefficients for TNB at  $T_g$  (342 K).

| Sample        | Third harmonic                         |                               | Fifth harmonic                         |                               |
|---------------|--|-------------------------------|--|-------------------------------|
|               | $D$<br>( $\times 10^{-18}$ cm $^2$ /s) | $q'$<br>( $\text{\AA}^{-1}$ ) | $D$<br>( $\times 10^{-18}$ cm $^2$ /s) | $q'$<br>( $\text{\AA}^{-1}$ ) |
| July 2005     | 9                                      | 0.028                         | 8                                      | 0.046                         |
| February 2005 | 10                                     | 0.029                         | 8                                      | 0.048                         |
| July 2004     | 12                                     | 0.035                         | 7                                      | 0.058                         |

Thus we have used  $T_g - 6$  K ( $=336$  K) as our standard sample deposition temperature. We believe that such samples are essentially free of thermal history effects and thus represent the dynamics of TNB as an equilibrium supercooled liquid. A future publication will explore the origin of the very long induction times observed for samples deposited further below  $T_g$ .

One other potential artifact related to thermal history was explored. Following deposition at  $T_g - 6$  K, the samples were typically held at room temperature ( $\sim T_g - 50$  K) for several days before being annealed in the neutron beam line at  $T_g$ . While we cannot easily eliminate this storage at room temperature from our experimental protocol, we can make two arguments that this does not have an important effect on subsequent diffusion. First, we note that samples held at room temperature for one day and seven days show no significant difference in behavior. One sample was held at room temperature for 12 months. The unannealed structure was unchanged by this waiting time, and subsequent annealing of this sample produced a third harmonic peak decay that was just slightly slower (about 20%) than samples held for only a few days at room temperature. Second, we checked that the introduction of additional thermal cycles between  $T_g$  and room temperature had no effect on the observed diffusion. These data sets were indistinguishable from those that were measured during an uninterrupted annealing process, as illustrated in Fig. 10. The triangles show the third harmonic peak decay for a typical sample with continuous annealing. The squares show the behavior of a sample annealed at  $T_g$

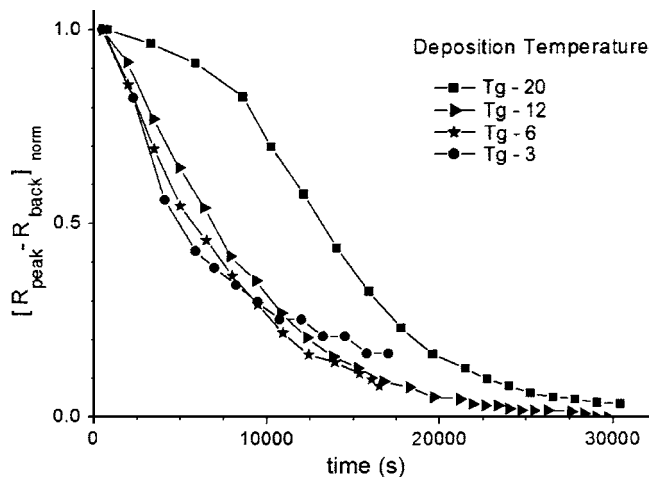


FIG. 9. Normalized intensity of the third harmonic Bragg peak for samples deposited at temperatures between  $T_g - 3$  (339 K) and  $T_g - 20$  (322 K). All samples were annealed at  $T_g$ . Deposition considerably below  $T_g$  results in slower dynamics.

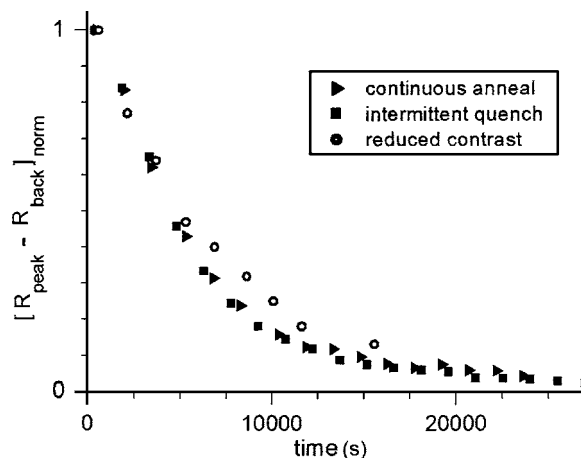


FIG. 10. Normalized intensity of the third harmonic peak for three samples deposited at  $T_g - 6$  K and annealed at  $T_g$ . The triangles are data for a sample which was continuously annealed while the squares are for a sample that was quenched to room temperature twice during the annealing process. Only time at  $T_g$  was counted in constructing this plot. Clearly quenching to room temperature has no effect on the observed dynamics. Open circles show data for a reduced contrast sample, in which  $h$ -TNB layers alternated with 1:1 mixed  $h$ -TNB/ $d$ -TNB layers. The observed dynamics are little affected by isotopic substitution.

1.5 h, then cooled to room temperature for 4 h, then returned to  $T_g$  for another 1.5 h, then cooled to room temperature for 26 h, and then returned to  $T_g$  for a final 4 h; only the time at  $T_g$  is used to construct the figure.

*Isotope influence.* While these neutron reflectivity experiments are strictly measuring the interdiffusion of  $h$ -TNB and  $d$ -TNB, control experiments justify our assumption that the different isotopes have very similar dynamics. Reduced contrast neutron reflectivity experiments were performed using a multilayer structure with  $h$ -TNB for one set of layers and a 1:1 mixture of  $h$ -TNB/ $d$ -TNB for the alternating layers. Figure 10 shows that the decay of the third harmonic for a reduced contrast sample is very similar to those of our typical full contrast samples. The small differences that appear at times larger than 5000 s are due to the smaller initial peak height in the reduced contrast sample. Fits like those shown in Fig. 6 have been performed for one reduced contrast sample and the best fit value of  $D$  was identical within experimental error to that obtained for the corresponding full contrast sample. Dielectric relaxation measurements have been performed on  $h$ -TNB and  $d$ -TNB by Richert *et al.*<sup>40</sup> Based on these measurements, the difference in  $T_g$  values for these two molecules is 2 K. This small difference is qualitatively consistent with the evidence presented in this paragraph. (The dielectric measurements were consistent with the value of  $T_g = 342$  K for  $h$ -TNB used in this paper.<sup>43</sup>)

## DISCUSSION

It is important to compare these neutron reflectivity results to previous measurements of self-diffusion of TNB at  $T_g$ . Using a real-space ion beam technique forward recoil spectrometry (FRoS),  $D$  values have been reported over the temperature range  $T_g$  to  $T_g + 20$  K, with a value  $D = 1.6 \times 10^{-16}$  cm $^2$ /s reported at  $T_g$ .<sup>25</sup> These FRoS results showed a much weaker temperature dependence for translational diffu-

sion than that reported for the viscosity in the supercooled regime. This leads to an enhancement of diffusion by a factor of 400 relative to the Stokes-Einstein prediction at  $T_g$ .

The diffusion coefficient determined by FReS is about one decade larger than the values determined by neutron reflectivity. A possible explanation for this discrepancy is that the two measurements are performed on different length scales and that diffusion is not Fickian over this range of length scales. Non-Fickian diffusion gives rise to translational motion for which the effective diffusion coefficient changes with wave vector or length scale.

The FReS experiments have a spatial resolution of  $\sim 35$  nm and typically the root-mean-square displacement was larger than this value after annealing. Measurements at various annealing times indicated that the FReS results represent the true long-time diffusion coefficient (limit of  $q \rightarrow 0$ ). The effective length scale of these neutron reflectivity measurements is significantly less than in the FReS measurements. The third harmonic for our 30 nm multilayers decays in about  $10^4$  s; based upon the measured  $D$ , this corresponds to an rms displacement of about 5 nm.

Partly inspired by preliminary accounts of this work, recently several papers have appeared that discuss the crossover from the non-Fickian to Fickian diffusion in supercooled liquids.<sup>11,44,45</sup> A large crossover length (or small crossover  $q$ ) is associated with spatially heterogeneous dynamics, which are thought to be important in TNB based upon the significant enhancement of translational diffusion observed near  $T_g$ . From this perspective, the difference in  $D$  values obtained from FReS and neutron reflectivity can be qualitatively rationalized.

Although we report here that our neutron reflectivity results are consistent with Fickian diffusion when considering the decay of a particular Bragg peak (e.g., Fig. 6), we have also attempted to fit our data with a variety of non-Fickian diffusion models. These fits were also successful as long as  $I_s(q, t)$  in the non-Fickian model decays exponentially with time; thus our results are also consistent with some types of non-Fickian diffusion. Fits of the data to non-Fickian models yield the same diffusion coefficient at a given wave vector as was obtained from the Fickian model. Table I shows that the diffusion coefficients that we obtain from the fifth harmonic peaks (at higher values of  $q$ ) have systemically smaller  $D$  values than those obtained from the third harmonic peaks. This effect is marginally significant given the experimental error but it is consistent with the information from the FReS measurements in that lower  $q$  measurements are giving larger diffusion coefficients.

## CONCLUSION

We have reported the first measurements of translational motion in a deeply supercooled, single component glass former on the nanometer length scale. The self-part of the intermediate scattering function  $I_s(q, t)$  is found to decay exponentially. In the  $q$  range investigated, the neutron reflectivity data are suggestive of a  $q$  dependence in the diffusion coefficient. This trend, which is supported by comparison to previous diffusion measurements at smaller  $q$  values, is

qualitatively consistent with models of spatially heterogeneous dynamics. These experiments are being extended to cover a wider range of wave vectors and these data should prove very useful in understanding spatially heterogeneous dynamics and its influence on translational motion near  $T_g$ .

## ACKNOWLEDGMENTS

We gratefully acknowledge the support of NSF-Chemistry (02457674). We thank Walter Kob, Peter Harrowell, and Paul Kienzle for helpful conversations. We thank Lian Yu and Tian Wu for performing DSC measurements.

- <sup>1</sup>C. A. Angell, K. L. Ngai, G. B. McKenna, P. F. McMillan, and S. W. Martin, *J. Appl. Phys.* **88**, 3113 (2000).
- <sup>2</sup>P. G. Debenedetti and F. H. Stillinger, *Nature (London)* **410**, 259 (2001).
- <sup>3</sup>M. D. Ediger, C. A. Angell, and S. R. Nagel, *J. Phys. Chem.* **100**, 13200 (1996).
- <sup>4</sup>T. R. Kirkpatrick and P. G. Wolynes, *Phys. Rev. A* **35**, 3072 (1987).
- <sup>5</sup>V. Lubchenko and P. G. Wolynes, *J. Chem. Phys.* **119**, 9088 (2003).
- <sup>6</sup>K. S. Schweizer and E. J. Saltzman, *J. Chem. Phys.* **121**, 1984 (2004).
- <sup>7</sup>J. P. Garrahan and D. Chandler, *Proc. Natl. Acad. Sci. U.S.A.* **100**, 9710 (2003).
- <sup>8</sup>W. Gotze and L. Sjogren, *Z. Phys. B: Condens. Matter* **65**, 415 (1987).
- <sup>9</sup>D. R. Reichman and P. Charbonneau, *J. Stat. Mech.: Theory Exp.* 2005, P05013.
- <sup>10</sup>G. Szamel, *Phys. Rev. Lett.* **90**, 228301 (2003).
- <sup>11</sup>L. Berthier, *Phys. Rev. E* **69**, 020201 (2004).
- <sup>12</sup>K. Binder, *J. Non-Cryst. Solids* **307**, 1 (2002).
- <sup>13</sup>C. Donati, S. C. Glotzer, P. H. Poole, W. Kob, and S. J. Plimpton, *Phys. Rev. E* **60**, 3107 (1999).
- <sup>14</sup>J. Horbach and W. Kob, *J. Phys.: Condens. Matter* **14**, 9237 (2002).
- <sup>15</sup>D. N. Perera and P. Harrowell, *J. Chem. Phys.* **111**, 5441 (1999).
- <sup>16</sup>S. Sastry, P. G. Debenedetti, and F. H. Stillinger, *Nature (London)* **393**, 554 (1998).
- <sup>17</sup>A. Schob, F. Cichos, J. Schuster, and C. von Borczyskowski, *Eur. Polym. J.* **40**, 1019 (2004).
- <sup>18</sup>C. Y. Wang and M. D. Ediger, *J. Phys. Chem. B* **103**, 4177 (1999).
- <sup>19</sup>E. V. Russell and N. E. Israeloff, *Nature (London)* **408**, 695 (2000).
- <sup>20</sup>K. Schmidt-Rohr and H. W. Spiess, *Phys. Rev. Lett.* **66**, 3020 (1991).
- <sup>21</sup>U. Tracht, M. Wilhelm, A. Heuer, H. Feng, K. Schmidt-Rohr, and H. W. Spiess, *Phys. Rev. Lett.* **81**, 2727 (1998).
- <sup>22</sup>R. Richert, *J. Phys.: Condens. Matter* **14**, R703 (2002).
- <sup>23</sup>M. D. Ediger, *Annu. Rev. Phys. Chem.* **51**, 99 (2000).
- <sup>24</sup>H. Sillescu, *J. Non-Cryst. Solids* **243**, 81 (1999).
- <sup>25</sup>S. F. Swallen, P. A. Bonvallet, R. J. McMahon, and M. D. Ediger, *Phys. Rev. Lett.* **90**, 015901 (2003).
- <sup>26</sup>M. K. Mapes, S. F. Swallen, and M. D. Ediger, *J. Phys. Chem. B* **110**, 507 (2006).
- <sup>27</sup>C. T. Thurau and M. D. Ediger, *J. Chem. Phys.* **118**, 1996 (2003).
- <sup>28</sup>A. Veniaminov, H. Sillescu, and E. Bartsch, *J. Chem. Phys.* **122**, 174902 (2005).
- <sup>29</sup>C. Y. Wang and M. D. Ediger, *J. Phys. Chem. B* **104**, 1724 (2000).
- <sup>30</sup>I. Koper, M. C. Bellissent-Funel, and W. Petry, *J. Chem. Phys.* **122**, 014514 (2005).
- <sup>31</sup>A. Tolle, J. Wuttke, H. Schober, O. G. Randl, and F. Fujara, *Eur. Phys. J. B* **5**, 231 (1998).
- <sup>32</sup>C. R. Bartels, B. Crist, and W. W. Graessley, *Macromolecules* **17**, 2702 (1984).
- <sup>33</sup>E. Sivaniah, R. A. L. Jones, and M. Sferazza, *Phys. Rev. E* **67**, 052801 (2003).
- <sup>34</sup>S. M. Baker, G. S. Smith, N. J. S. Brown, M. Nastasi, and K. Hubbard, *Phys. Rev. B* **55**, 7255 (1997).
- <sup>35</sup>M. Gupta, A. Gupta, J. Stahn, M. Horisberger, T. Gutberlet, and P. Al-lenspach, *Phys. Rev. B* **70**, 184206 (2004).
- <sup>36</sup>C. M. Whitaker and R. J. McMahon, *J. Phys. Chem.* **100**, 1081 (1996).
- <sup>37</sup>All interfacial widths given in this paper are the full width at half maximum values for the derivative of the interfacial profile.
- <sup>38</sup>I. Chang and H. Sillescu, *J. Phys. Chem. B* **101**, 8794 (1997).
- <sup>39</sup>X. L. Zhou and S. H. Chen, *Phys. Rep.* **257**, 223 (1995).
- <sup>40</sup>R. Richert, K. Duvvuri, and L.-T. Duong, *J. Chem. Phys.* **118**, 1828 (2003).

<sup>41</sup>X. R. Zhu and C. H. Wang, J. Chem. Phys. **84**, 6086 (1986).

<sup>42</sup>K. Zemke, K. Schmidt-Rohr, J. H. Magill, H. Sillescu, and H. W. Spiess, Mol. Phys. **80**, 1317 (1993).

<sup>43</sup>J. H. Magill, J. Chem. Phys. **47**, 2802 (1967).

<sup>44</sup>L. Berthier, D. Chandler, and J. P. Garrahan, Europhys. Lett. **69**, 320 (2005).

<sup>45</sup>K. S. Schweizer and E. J. Saltzman, J. Phys. Chem. B **108**, 19729 (2004).